AD-A096 232 CINCINNATI UNIV OH DEPT OF AEROSPACE ENGINEERING AND--ETC F/G 20/4
THREE-DIMENSIONAL SUPERSONIC VISCOUS FLOW OVER A CONE AT INCIDE--ETC(U)
JAN 81 A LIN, S G RUBIN N00014-79-C-0849
UNCLASSIFIED NL

END
DATE FILMED
4-81
DTIC

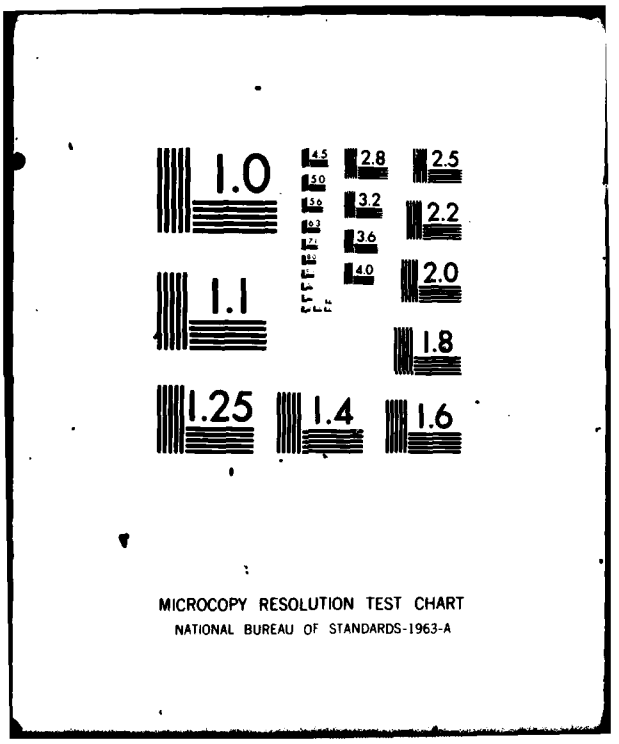
1.0
1.1
1.25
1.4
1.6
1.8
2.0
2.2
2.5
2.8
3.2
3.6
4.0
4.5
5.0
5.6
6.3
MICROCOPY RESOLUTION TEST CHART
NATIONAL BUREAU OF STANDARDS-1963-A

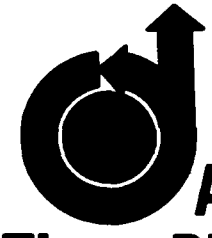

AIAA-81-0192
Three-Dimensional Supersonic Viscous Flow Over a Cone at Incidence

A. Lin and S.G. Rubin,
University of Cincinnati, Ohio

AIAA 19th AEROSPACE SCIENCES MEETING

January 12-15, 1981/St. Louis, Missouri

THREE-DIMENSIONAL SUPERSONIC VISCOUS FLOW OVER A CONE AT INCIDENCE

A. Lin* and S.G. Rubin**

University of Cincinnati
Cincinnati, Ohio 45221

Abstract

The viscous supersonic flow over a sharp cone at incidence is examined numerically with a coupled strongly implicit algorithm for the properties in the plane normal to the cone axis. The Navier-Stokes equations are considered in a boundary layer-like or parabolized manner and global relaxation is considered for the pressure interaction. It is shown that departure effects can be effectively eliminated by forward differencing for the axial pressure gradient. Moreover, this approximation retains the implicit free pressure interaction required for geometries where axial flow separation is possible.

1. Introduction

For a significant class of geometric configurations and flow conditions solutions of the full Navier-Stokes equations can be approximated quite accurately with boundary layer like marching techniques in thin viscous layers, coupled with relaxation or marching procedures for inviscid sub- and supersonic regions, respectively. For large Reynolds number flows this approach has been developed in several ways, e.g., interacting boundary layer theory,[1] parabolized Navier-Stokes (PNS) theory,[2] viscous or single layer theory[3] and two-layer interactive theory.[4] Single sweep marching for supersonic outer flows with little or no upstream interaction, and global or multiple pass methods when upstream influence, including possible separation, is an important feature of the flow have been discussed for a variety of problems. References 2 and 3 review much of the earlier work on this subject.

The present study is concerned with the analysis of a global approach to the Navier-Stokes equations and a single sweep PNS application for the supersonic laminar flow over a sharp cone geometry. This geometry has been examined extensively during the past decade and in view of the variety of complex flow phenomena associated with the cone at incidence, it has served as a prototype for analysis of new computational methods. Of particular interest here are procedures that allow for the evaluation of such a configuration at relatively large angles of incidence. In particular, we are concerned with the accurate prediction of the secondary flow vortex patterns, imbedded shock formation, axial and secondary flow pressure interaction, and finally the surface pressure and heat transfer.

The secondary flow interaction with shocks and vortex formation is non-trivial and therefore a coupled strongly implicit (CSIP) algorithm, developed previously for the incompressible Navier-Stokes equations,[5] is applied here in order to provide a "two-dimensional" coupling for the three velocity components. The secondary flow pressure and temperature gradients remain uncoupled in order to limit computer storage requirements; however, the latter is evaluated with the strongly implicit (SIP) algorithm. The outer shock boundary conditions are completely coupled into the CSIP algorithm.

The continuity and normal momentum equations are related to the evaluation of the normal velocity and pressure, respectively. This is contrary to most conventional Navier-Stokes and PNS procedures. However, it is consistent with the boundary layer and thin shock layer techniques that have been applied in non-interactive analyses. A deferred-corrector is applied to the upwind or boundary layer approximation used in the initial marching sweep for the axial (ξ) convection terms. This K-R[6] corrector provides a stable second-order accurate approximation for the global marching procedure.

As a peripheral aspect of the present study several difference approximations for the axial pressure gradient term p_ξ appearing in the ξ-momentum equation are considered. This term controls the "elliptic" pressure interaction[2] and can produce the so-called departure instability indicative of the upstream pressure effect. It is seen that with an appropriate forward difference approximation to p_ξ, the departure effect is suppressed and a consistent, stable, pressure interactive procedure, tested previously for incompressible flows, is also applicable for the cone calculations. Since there is not strong upstream interaction for the sharp cone geometry this has little effect on the solutions; however, it does provide a basis for further consideration with other configurations.

Solutions are presented for several cases; however, the major emphasis here is on the Tracy 10° half-angle cone[7] and the Marcillat[9] 9° half-angle cone. Incidence angles of from zero to 45° are considered.

---

* Research Assistant Professor, Department of Aerospace Engineering and Applied Mechanics. Member AIAA.

** Professor, Department of Aerospace Engineering and Applied Mechanics. Associate Fellow AIAA.

	TRACY	MARCILLAT	
HALF CONE ANGLE	10°	9°	
FREE STREAM REYNOLDS NO.	1.13×10^6/ft	1.09×10^5/cm	0.251×10^5/cm
FREE STREAM MACH NO.	7.95	6.845	6.675
WALL TEMPERATURE	558°R	295°K	
STAGNATION TEMPERATURE	1360°R	600°K	
WALL TEMP./ STAG. TEMP.	0.41	0.49	
CONSTANT Pr	0.75	0.75	
γ	1.4	1.4	
COMPARING TO DATA IS DONE FOR x =	0.33ft, 0.286 ft	5.5, 6.0, 9.5, 13.0, 13.5, 17.0, 19.0, 17.5, 21.5 cm	

TABLE 1: FLOW CONDITIONS

2. Governing Equations

The full steady Navier-Stokes equations are considered for the global relaxation procedure. However, for the infinite cone geometry considered here only a single marching sweep is required as upstream interaction is negligible. Therefore the axial diffusion terms and K-R second-order corrector have not been introduced in the initial step. For other configurations, where multiple relaxation sweeps are required, these terms would be introduced; although, even then their importance may be questionable.

A surface oriented coordinate system is considered (Fig. 1); x is measured along the cone generators; y is normal to the surface, and ϕ is the circumferential or azimuthal angle; $\phi = 0,\pi$ at the wind- and lee planes, respectively.

In this coordinate frame the governing conservation equations are as follows:

continuity:

$$\frac{\partial\rho}{\partial t} + \frac{\partial}{\partial x}(\rho u) + \frac{\partial}{\partial y}(\rho v) + \frac{1}{r}\frac{\partial}{\partial\phi}(\rho w) + \frac{\rho}{r}(u\sin\theta + v\cos\theta) = 0 \qquad (1a)$$

x-momentum:

$$\frac{\partial u}{\partial t} + u\frac{\partial u}{\partial x} + v\frac{\partial u}{\partial y} + \frac{w}{r}\frac{\partial u}{\partial\phi} - \frac{w^2\sin\theta}{r} = -\frac{1}{\rho}\frac{\partial P}{\partial x} + \frac{1}{\rho}\{\frac{4}{3}\frac{\partial}{\partial x}(\mu\frac{\partial u}{\partial x}) - \frac{2}{3}\frac{\partial}{\partial x}(\mu\frac{\partial v}{\partial y}) + \frac{\partial}{\partial y}(\mu\frac{\partial v}{\partial x}) + \frac{\partial}{\partial y}(\mu\frac{\partial u}{\partial y}) + \frac{1}{r^2}\frac{\partial}{\partial\phi}(\mu\frac{\partial u}{\partial\phi}) + \frac{4\sin\theta}{3r}\mu\frac{\partial u}{\partial x} + \frac{\mu\cos\theta}{r}\frac{\partial u}{\partial y} + \frac{\mu\cos\theta}{3r}\frac{\partial v}{\partial x} + \frac{1}{r}\frac{\partial\mu}{\partial\phi}\frac{\partial w}{\partial x} - (\frac{2}{3r}\frac{\partial\mu}{\partial x} + \frac{4\mu}{3r}\sin\theta)(u\sin\theta + v\cos\theta) + \frac{4\sin\theta}{3r}\mu\frac{\partial u}{\partial x} + \frac{\mu\cos\theta}{r}\frac{\partial u}{\partial y} + \frac{\mu\cos\theta}{3r}\frac{\partial v}{\partial x} + \frac{1}{r}\frac{\partial\mu}{\partial\phi}\frac{\partial w}{\partial x} - (\frac{7\sin\theta}{3r^2}\mu + \frac{2}{3r}\frac{\partial\mu}{\partial x})\frac{\partial w}{\partial\phi} + \frac{\mu}{3r}\frac{\partial^2 w}{\partial x\partial\phi} - \frac{\sin\theta}{r^2}\frac{\partial\mu}{\partial\phi}w\} \qquad (1b)$$

y-momentum:

$$\frac{\partial v}{\partial t} + u\frac{\partial v}{\partial x} + v\frac{\partial v}{\partial y} + \frac{w}{r}\frac{\partial v}{\partial\phi} - \frac{w^2\cos\theta}{r} = -\frac{1}{\rho}\frac{\partial P}{\partial y} + \frac{1}{\rho}\{\frac{4}{3}\frac{\partial}{\partial y}(\mu\frac{\partial v}{\partial y}) + \frac{\partial}{\partial x}(\mu\frac{\partial v}{\partial x}) + \frac{\partial\mu}{\partial x}\frac{\partial u}{\partial y} - \frac{2}{3}\frac{\partial\mu}{\partial y}\frac{\partial u}{\partial x} + \frac{\mu}{3}\frac{\partial^2 u}{\partial x\partial y} + \frac{1}{r^2}\frac{\partial}{\partial\phi}(\mu\frac{\partial v}{\partial\phi}) + \frac{4\mu\cos\theta}{3r}\frac{\partial v}{\partial y} + \frac{\mu\sin\theta}{r}\frac{\partial v}{\partial x} - \frac{4\mu\cos\theta}{3r^2}(u\sin\theta + v\cos\theta) - \frac{2\sin\theta}{3r}\frac{\partial\mu}{\partial y}u + \frac{\mu\sin\theta}{3r}\frac{\partial u}{\partial y} - \frac{2\cos\theta}{3r}\frac{\partial\mu}{\partial y}v + \frac{1}{r}\frac{\partial\mu}{\partial\phi}\frac{\partial w}{\partial y} - (\frac{7\mu\cos\theta}{3r^2} + \frac{2}{3r}\frac{\partial\mu}{\partial y})\frac{\partial w}{\partial\phi} + \frac{\mu}{3r}\frac{\partial^2 w}{\partial y\partial\phi} - \frac{\cos\theta}{r^2}\frac{\partial\mu}{\partial\phi}w\} \qquad (1c)$$

ϕ-momentum:

$$\frac{\partial w}{\partial t} + u\frac{\partial w}{\partial x} + v\frac{\partial w}{\partial y} + \frac{w}{r}\frac{\partial w}{\partial\phi} + \frac{w}{r}(u\sin\theta + v\cos\theta) = -\frac{1}{\rho r}\frac{\partial P}{\partial\phi} + \frac{1}{\rho}\{\frac{\partial}{\partial x}(\mu\frac{\partial w}{\partial x}) + \frac{\partial}{\partial y}(\mu\frac{\partial w}{\partial y}) + \frac{4}{3r^2}\frac{\partial}{\partial\phi}(\mu\frac{\partial w}{\partial\phi}) + \frac{1}{r}\frac{\partial\mu}{\partial x}\frac{\partial u}{\partial\phi} + \frac{1}{r}\frac{\partial\mu}{\partial y}\frac{\partial v}{\partial\phi} - \frac{2}{3r}\frac{\partial\mu}{\partial\phi}(\frac{\partial u}{\partial x} + \frac{\partial v}{\partial y}) + \frac{\mu}{3r}(\frac{\partial^2 u}{\partial x\partial\phi} + \frac{\partial^2 v}{\partial y^2}) + \frac{7\mu}{3r^2}(\frac{\partial u}{\partial\phi}\sin\theta + \frac{\partial v}{\partial\phi}\cos\theta) + \frac{4}{3r^2}\frac{\partial\mu}{\partial\phi}(u\sin\theta + v\cos\theta) +$$

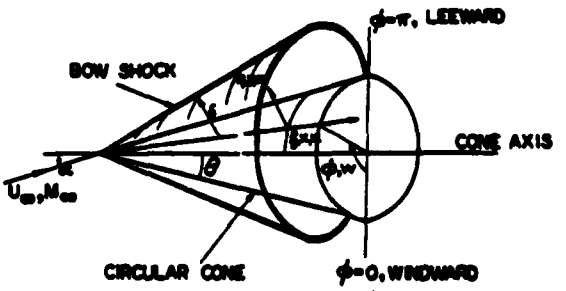

Fig. 1. Flow Geometry.

$$+ \frac{\mu}{r}\left(\frac{\partial w}{\partial x}\sin\theta + \frac{\partial w}{\partial y}\cos\theta\right) - \left(\frac{\mu}{r^2} + \frac{\cos\theta}{r}\frac{\partial \mu}{\partial y}\right.$$

$$\left. + \frac{\sin\theta}{r}\frac{\partial \mu}{\partial x}\right) w\Big\} \qquad (1d)$$

Energy-equation:

$$\rho \frac{\partial}{\partial t}(C_p T) + \rho u \frac{\partial}{\partial x}(C_p T) + \rho v \frac{\partial}{\partial y}(C_p T)$$

$$+ \frac{\rho w}{r}\frac{\partial}{\partial \phi}(C_p T)$$

$$= \frac{\partial P}{\partial t} + u\frac{\partial P}{\partial x} + v\frac{\partial P}{\partial y} + \frac{w}{r}\frac{\partial P}{\partial \phi}$$

$$+ \frac{\partial}{\partial x}\left(k\frac{\partial T}{\partial x}\right) + \frac{\partial}{\partial y}\left(k\frac{\partial T}{\partial y}\right) + \frac{1}{r}\frac{\partial}{\partial \phi}\left(\frac{k}{r}\frac{\partial T}{\partial \phi}\right)$$

$$+ \frac{k}{r}\left(\frac{\partial T}{\partial x}\sin\theta + \frac{\partial T}{\partial y}\cos\theta\right) + \frac{4\mu}{3}\left[\left(\frac{\partial u}{\partial x}\right)^2 + \left(\frac{\partial v}{\partial y}\right)^2 - \frac{\partial u}{\partial x}\frac{\partial v}{\partial y}\right]$$

$$+ \frac{4\mu}{3r^2}\left[u\sin\theta + v\cos\theta + \frac{\partial w}{\partial \phi}\right]^2$$

$$+ \mu\left(\frac{\partial u}{\partial y} + \frac{\partial v}{\partial x}\right)^2 + \mu\left[\left(\frac{1}{r}\frac{\partial u}{\partial} + \frac{\partial w}{\partial x} - \frac{w\sin\theta}{r}\right)^2\right.$$

$$\left. + \left(\frac{1}{r}\frac{\partial v}{\partial \phi} + \frac{\partial w}{\partial y} - \frac{w\cos\theta}{r}\right)^2\right]$$

$$- \frac{4\mu}{3r}\left(u\sin\theta + v\cos\theta + \frac{\partial w}{\partial \phi}\right)\left(\frac{\partial u}{\partial x} + \frac{\partial v}{\partial y}\right) \qquad (1e)$$

where θ is the half-cone angle and $r = x\sin\theta + y\cos\theta$. In addition, the state equation and viscosity-temperature and thermal conductivity-temperature relations close the system. The Sutherland law is used for $\mu = \mu(T)$ and the Prandtl number $Pr = \mu C_p/K$ is constant.

The system (1) is non-dimensionalized with the shock layer thickness $\delta(x,\phi)$ so that $\eta = y/\delta$; $\xi = x$ and $\phi = \phi$. The velocities are normalized with the free stream U_∞, ρ with ρ_∞, p with $\rho_\infty U_\infty^2$, T with U_∞^2/C_{p_∞}. The unit Reynolds number $Re = \rho_\infty U_\infty/\mu_\infty$. The system (1) is then transformed from (ξ,η,ϕ) to (x,y,ϕ) coordinates. The respective velocities are (u,v,w). It is significant that in the course of this transformation

$$\frac{\partial}{\partial x} = \frac{\partial}{\partial \xi} - \frac{\eta}{\delta}\delta_\xi \frac{\partial}{\partial \eta} \qquad (2a)$$

and

$$\frac{\partial}{\partial \phi} = \frac{\partial}{\partial \theta} - \frac{\eta}{\delta}\delta_\phi \frac{\partial}{\partial \eta} \qquad (2b)$$

Although the pressure will be uncoupled from the (u,v,w) CSIP algorithm, the p_x and p_ϕ terms do couple partially through the p_η contributions in (2). This term can be eliminated, with the normal momentum equation (1c), in terms of (u,v,w). In fact, for inviscid conical flow $\partial/\partial\xi \equiv 0$ and therefore we would expect the role of p_ξ to be relatively minor. The other ξ-derivatives are not negligible in the boundary layer and possibly in the outer layer for larger incidence angles.

The final system of equations is quite formidable and will be given in a separate report. In order to allow for subsequent code debugging, error correction or future modifications in the difference equations or relaxation procedure, each term in each equation is introduced into the coefficients of the differenced and quasilinearized form independently. Therefore each contribution is identifiable and easily located.

3. Difference Equations

The final transformed equations are differenced as follows: conventional central differencing for the η and ϕ derivatives in the axial (ξ) and azimuthal (ϕ) momentum and energy equations, see figure 2 for a description of the difference grid.

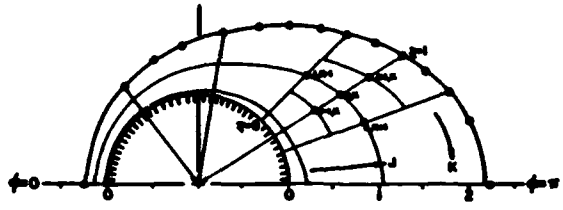

Fig. 2. Difference Grid in the Cross Plane.

The axial convective derivatives $\partial/\partial\xi$ are upwind differenced, with a K-R corrector inserted for multiple sweep applications; i.e.,

$$(u_\xi)_i = \left(\frac{u_i - u_{i-1}}{\Delta\xi}\right)PL + \frac{u_{i+1} - u_i}{\Delta\xi}(1-PL)$$

$$+ \frac{u^*_{i+1} - 2u^*_i + u^*_{i-1}}{2\Delta\xi}(2PL-1)$$

where $PL = 1$ for $u_i > 0$; $PL = 0$ for $u_i < 0$. The superscript (*) denotes solutions from the previous global iteration. These are assumed to be zero in the initial marching sweep.

The continuity and normal momentum equations, as noted previously, are considered in the boundary layer or thin shock layer manner as first-order equations for v and p, respectively and are differenced at the half-point $\eta_j + (\Delta\eta/2)_j$ with the trapezoidal rule. When the p_η term from the η momentum equation is used in (2a) and (2b), conventional central differences are applied for the coupled velocity derivatives that are introduced into the ξ and ϕ momentum equations.

The final system of difference equations are quasi-linearized to provide the familiar second-order approximation

$$f\,g = f^*g + g^*f - f^*g^*$$

where the superscript (*) here denotes the previous iteration at the axial ξ_i location. Strictly speaking if ξ_{i-1} values are used this approximation

remains second-order and is then non-iterative.

4. Numerical Algorithm and Solution Procedure

After differencing, substitution of p_η and quasi-linearization, the final system to be evaluated is of the following form for (u,v,w) at $\xi = \xi_i$:

ξ,ϕ momentum:

$$E_{\ell u_{j,k}} U_{j+1,k} + W_{\ell u_{j,k}} U_{j-1,k} + N_{\ell u_{j,k}} U_{j,k+1} + S_{\ell u_{j,k}} U_{j,k-1} + P_{\ell u_{j,k}} U_{j,k} + E_{\ell w_{j,k}} W_{j+1,k} + W_{\ell w_{j,k}} W_{j-1,k} + N_{\ell w_{j,k}} W_{j,k+1} + S_{\ell w_{j,k}} W_{j,k-1} + P_{\ell w_{j,k}} W_{j,k} + W_{\ell r_{j,k}} V_{j-1,k} + P_{\ell v_{j,k}} V_{j,k} + E_{\ell v_{j,k}} V_{j+1,k} + F_{\ell_{j,k}} = 0 \quad (3a)$$

where $\ell = 2, 3$ for ξ,ϕ equations respectively.

continuity:

$$V_{j,k} = W_{1v_{j,k}} V_{j-1,k} + P_{1u_{j,k}} u_{j,k} + W_{1u_{j,k}} U_{j-1,k} + P_{1w_{j,k}} W_{j,k} + W_{1w_{j,k}} W_{j-1,j} + N_{1w_{j,k}} W_{j,k+1} + S_{1w_{j,k}} W_{j,j-1} + WN_{1w_{j,k}} W_{j-1,k+1} + WS_{1w_{j,k}} W_{j-1,k-1} + F_{1_{j,k}} = 0 \quad (3b)$$

The coupled strongly implicit (CSIP) algorithm is of the form[5]

$$U_{j,k} = A_{11_{j,k}} U_{j-1,k} + A_{12_{j,k}} U_{j,k+1} + B_{11_{j,k}} W_{j-1,k} + B_{12_{j,k}} W_{j,k+1} + C_{1_{j,k}} V_{j-1,k} + D_{1_{j,k}} \quad (4a)$$

$$W_{j,k} = A_{21_{j,k}} U_{j-1,k} + A_{22_{j,k}} U_{j,k+1} + B_{21_{j,k}} W_{j-1,k} + B_{22_{j,k}} W_{j,k+1} + C_{2_{j,k}} V_{j-1,k} + D_{2_{j,k}} \quad (4b)$$

and the continuity equation (3b) where the corner points $W_{j-1,k+1}$ are treated implicitly. The algorithm is structured to evaluate all k values before proceeding from j to j+1.

This is a (2x2)+1 matrix system and not a much larger (3x3) system. The algorithms (4a) and (4b) are used in (3a,b) to eliminate $U_{j+1,k}$, $W_{j+1,k}$, $U_{j,k-1}$, $W_{j,k-1}$. The corner points j+1, k+1 are treated explicitly in obtaining the recursion relationships for the coefficients in (4a), (4b). See reference 5 for a matrix description of the CSIP algorithm. These are obtained by directly relating (3a,b) to (4a,b). The final recursion relationships are given in Appendix A. The boundary conditions for u, v, w, to be discussed in the following section, are coupled implicitly into the CSIP algorithm.

The energy equation which is of the form (3a) is solved independently with the SIP algorithm (4a). This is obtained by replacing u with T and setting v,w = 0 in (3a) and (4a) and inserting the appropriate coefficients from the transformed (1a). The pressure is obtained from the transformed normal momentum equation (1c) by integrating from the shock to the surface with the trapezoidal rule.

The procedure can be summarized as follows: (1) (u,v,w) are solved with the CSIP algorithm and coupled boundary conditions with ρ, T, p prescribed (p_η has been substituted from momentum into the ξ,ϕ momentum equations and is thereby implicit); (2) With the new shock values for p and T, T is updated with the SIP algorithm and p from the normal momentum equation. The viscosity and thermal conductivity coefficients and ρ are also updated; (3) With the new ρ, p, T, μ, k values, return to step (1) and continue until a convergence criterion is satisfied. A flow chart for the entire procedure is given in Appendix B.

This describes completely the evaluation at each location $\xi = \xi_i$ for a single sweep marching procedure. If additional sweeps are necessary, i.e., when pressure interaction and upstream influence are important, the process is repeated from the initial $\xi = \xi_0$ location and the KR correctors, axial diffusion, forward p_ξ difference terms dependent on the previous pass are updated. Multiple pass calculations have only been considered to a limited extent and these will not be discussed further here.

5. Boundary and Initial Conditions

Initial conditions are obtained directly from the governing difference equations by applying the numerical algorithm with $\partial/\partial\xi \equiv 0$; i.e., a conical flow approximation. Inviscid or step profiles with no-slip surface conditions are assumed to start this calculation. This procedure works well for incidence angles up to 10°. For $\alpha > 10°$, the 10° results are used as initial conditions and the exact α boundary conditions are imposed at the first marching step. The effect of the initial conditions rapidly vanishes as the shock layer is extremely small near the tip of the cone. It should be noted that while the $\partial/\partial\xi = 0$ solutions are reasonable approximations for the viscous cone flow, the exact solutions are noticeably different both in the viscous boundary layer and in the outer vertical region near the

lee plane. This is not surprising as the viscous behavior does not scale conically, i.e., as $\delta(x,\phi)$.

The boundary conditions at the surface $\eta = 0$ are $u = v = w = 0$ and $T = T_w$. At the outer shock wave $\eta = 1$, the Rankine-Hugoniot conditions apply:

mass conservation:

$$(u_1 - \rho u)\delta_\xi + \frac{1}{r}(w_1 - \rho w)\delta_\phi - (v_1 - \rho v) = 0 \qquad (5a)$$

tangential momentum:

$$(w_1 - w) + \frac{1}{r}\delta_\phi (V_1 - V) = 0 \qquad (5b)$$

$$(u_1 - u) + \delta_\xi (V_1 - V) = 0 \qquad (5c)$$

normal momentum:

$$\rho = \frac{\gamma+1}{\gamma-1 + \frac{2}{M_{n_1}^2}} \qquad (5d)$$

where subscript (1) denotes free stream components at the shock wave and M_{n_1} is the free stream normal Mach number which is a function of δ_ξ, δ_ϕ. The four equations (5a-d) coupled with the continuity equation (1a) evaluated at the half-point $\eta = 1 - \frac{\Delta\eta}{2}$ give five equations for the five unknowns, u, v, w, ρ, δ_ξ. The direction cosine δ_ϕ is not coupled but is treated iteratively with ρ and T which are only functions of M_{n_1} from the Rankine Hugoniot conditions. The coupled u, v, w boundary conditions are incorporated implicitly into the CSIP algorithm. The system (5) is quasi-linearized in the same manner as that for the interior equations. The combination of the Rankine-Hugoniot conditions and the coupled continuity equation ensure that global mass conservation is maintained. The final form of the outer boundary conditions includes (5b), which is linear since δ_ϕ is treated explicitly, and (5a,c,d) are combined to give

$$\frac{1}{2}M_\infty^2 [1 - (u_1 u + v_1 v + w_1 w)][(r-1)$$

$$+ (2-)(u_1 u + v_1 v + w_1 w) + (u^2 + v^2 + w^2)]$$

$$= [1 - 2(u_1 u + v_1 v + w_1 w) + (u^2 + v^2 + w^2)] \qquad (5e)$$

This equation is also quasi-linearized. In this form the stream function solution, appearing in the original system, has been eliminated.

This CSIP and SIP procedures are convergent to 10^{-10} for all incidence angles. The pressure equation is converged to 10^{-7} for $\alpha \leq 32°$. For $\alpha > 32°$ the pressure solution exhibits a slow divergence that is apparently associated with the explicit or uncoupled character of the normal momentum equation. If the pressure field is underrelaxed by including a time-like term in the normal momentum and energy equations, this divergence is suppressed and the overall system converges; however, the underrelaxation is very expensive computationally and it is evident that coupling the pressure directly would be more desirable.

The solutions for $\alpha > 30°$ depict fairly strong imbedded shock waves and significant vortex lift-off; therefore, the secondary flow pressure interaction will be quite strong and an implicit treatment of this effect may be required. We recall that the p_η contribution in (2b) is already introduced implicitly; however, the p_ϕ and δ_ϕ effects are considered iteratively.

Finally, symmetry conditions $u_\phi = v_\phi = T_\phi = p_\phi = 0$ and $w_{\phi\phi} = 0$ are imposed at the lee and wind planes. These conditions are coupled implicitly into the CSIP and SIP algorithms by appropriately modifying the coefficients of the difference equations at these locations; e.g., $u_{k+1} = u_{k-1}$ at $k = 1$, therefore $S_{\ell u_{j,k}} = 0$ in (3a,b) and $N_{\ell u_{j,k}}$ is modified to include the U_{k+1} coefficient so that $N_{\ell u_{j1}} = N_{\ell u_{j1}} + S_{\ell u_{j1}}$, etc.

6. Pressure Interaction and Departure

For any sweep of a one-step or global relaxation procedure the appropriate treatment of the pressure interaction term p_x in the axial momentum equations (1b) is essential. Even for supersonic free streams an "elliptic" pressure interaction is transmitted upstream through the p_x term when regions of subsonic flow, as in the wall boundary layer, are present. If p_x is prescribed the equations are truly parabolic and the upstream effect is lost. However, for flows where upstream effects are significant, if the p_x term is backward differenced in any form the interaction is included in the system.[2,8] This is manifested in the appearance of departure curves or instabilities whenever $\Delta x \geq (\Delta x)_{min}$, which is of the order of the thickness of the subsonic layer or $O(Re^{-1/2})$ for the viscous cone flow.[2] Therefore, in the present application, with $Re \gg 1$, reasonably accurate solutions are possible even for $\Delta x \ll (\Delta x)_{min}$.

This procedure is however inconsistent and for flows with significant pressure interaction may be inadequate. A global relaxation procedure is required if the inconsistency is to be eliminated. Moreover, in the global procedure it is necessary that each marching sweep be departure free and yet allow for an implicit pressure interaction in order to circumvent the separation point singularity that arises with an explicit pressure representation. In an earlier incompressible PNS thin layer study,[2,8] it was shown that forward p_ξ differencing is departure free and stable globally. Central p_ξ is unstable globally and backward p_ξ is not departure free. It was shown in references 2 and 8 that with forward p_ξ differencing, it was possible to march through separation regions departure free in each global relaxation sweep. This procedure was also tested for the cone calculations and the earlier conclusions obtained both analytically and numerically were verified. Although this effect is relatively

unimportant for cone flows where solutions with $\Delta x > (\Delta x)_{min}$ are acceptable except very close to the tip, for more complex configurations this procedure is considered important.

For the cone calculations, detailed tests for the value of $(\Delta x)_{min}$ as a function of Re have been considered. The resulting stability curve for $\alpha = 28°$ is shown in figure 3. This clearly confirms the earlier analysis and demonstrates that $(\Delta x)_{min}/y_{M=1}$ decreases as Re increases. The exact dependence is not proportional to $Re^{-1/2}$ as in the incompressible case. The use of a K-R second-order pressure correction for a forward-differenced p_x has not been addressed. Finally, we recall that the p_η contribution to p_x is treated implicitly and with a backward or marching mode for v_ξ; therefore, the entire global interaction is contained in p_ξ.

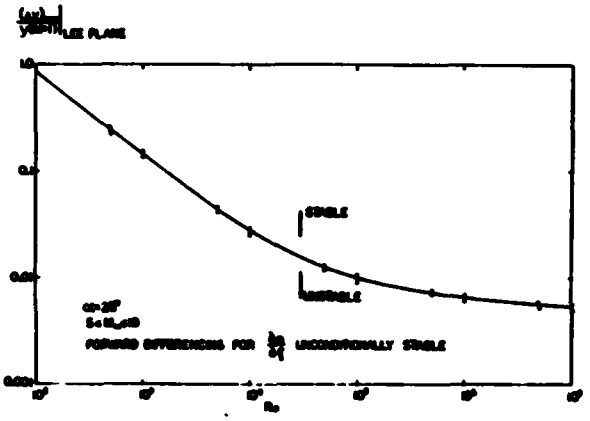

Fig. 3. Departure Condition with P_ξ Backward Differencing.

7. Results

Solutions have been obtained for two flow conditions for which experimental data is available[7,9] and for which numerical results have been obtained by PNS,[9-11] merged layer,[12] and boundary region[13] approximations. All the calculations were made with the CSIP algorithm for (u,v,w), the SIP algorithm for T and the trapezoidal rule for p. Converged solutions to a tolerance of 10^{-10} for successive iterations using double precision compilation on an AMDAHL 370-computer were obtained. Uniform grids were specified in η and ϕ. Calculations were run with both relatively coarse grids, e.g., 10 x 21, 19 x 31 and a finer 51 x 55 grid. For the finest grid calculation times were 0.0008 sec/CSIP Iteration/grid point. 7-15 CSIP iterations are required to converge the (u,v,w,δ_ξ) system. The CSIP procedure is called about 30-60 times to converge the pressure field. For $\alpha \geq 32°$ it takes about 30 minutes for the $(\partial/\partial\xi = 0)$ equations to converge and another 1 minute for any additional marching step.

Figure 4 shows the CPU time consumption as function of α to reach the same ξ location (= 2 ft) for Tracy conditions. From the figure it is seen that running time increases with α and due to underrelaxation required for $\alpha > 32°$, the times increase measurably. Double precision requires approximately four times that of single precision which runs about four times slower than a CDC 7600. Therefore we estimate conservatively that the maximum CPU requirement on a 7600 would be less than 25% of that of the AMDAHL computer if similar programming techniques were used. Non-uniform grids, in particular for the surface normal (η) direction, might reduce the overall computer time; however, for large incidence with imbedded shocks and lifting vortex motion the optimal grid distribution is not obvious.

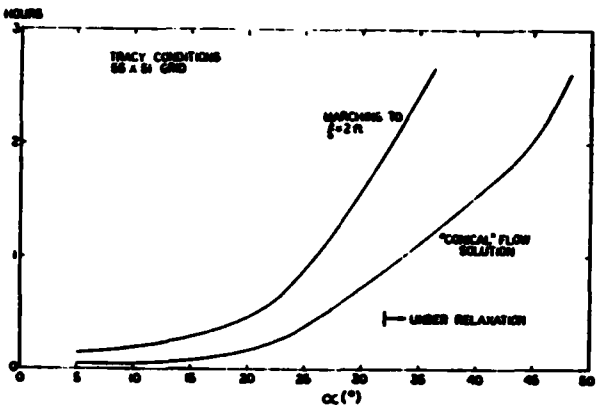

Fig. 4. CPU Time for Initial $(\frac{\partial}{\partial\xi} = 0)$ and Marching Solution.

Solutions have been obtained for incidence angles (α) up to 45° on a 10° half-angle (θ) cone, or $\alpha \leq 4.5\,\theta$. The interior shocks are captured, secondary flow separation regions are determined and vortex patterns are seen to lift far off the surface for large α.

Selected results are presented here primarily for the experimental conditions of Tracy[7] and Marcillat.[9] Some of the solutions are for very large incidence angles, where experimental data are unavailable. A 51 x 55 uniform grid is the finest mesh considered to date and therefore, we inject a note of caution for $\alpha > 32°$. In addition, as discussed previously, underrelaxation is required for these cases and further study of accuracy and convergence properties is required.

The heat transfer at the wind and lee planes for moderate to large angles of incidence is depicted in figures 5a,b. The agreement with the data is quite good as it is for the surface pressure distributions which are given in figures 6a,b,c. The effect of the imbedded secondary flow shock wave is apparent only for the largest incidence angles.

These effects can be seen somewhat more clearly in the $\alpha = 24°$ pitot pressure profiles and distributions of figures 7a,b,c. The significant change in p_0 across the shock layer is apparent. The stagnation pressure is affected by the inclination of the outer shock, the growth of

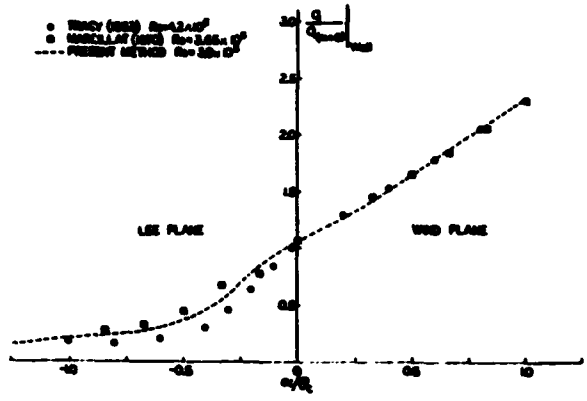

Fig. 5a. Symmetry Plane Heat Transfer - Moderate Incidence.

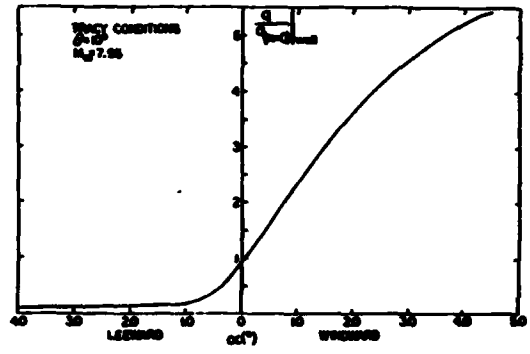

Fig. 5b. Symmetry Plane Heat Transfer - Large Incidence.

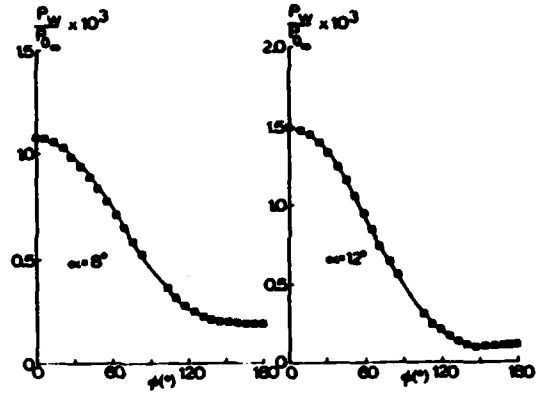

Fig. 6a. Surface Pressure at Moderate Incidence.

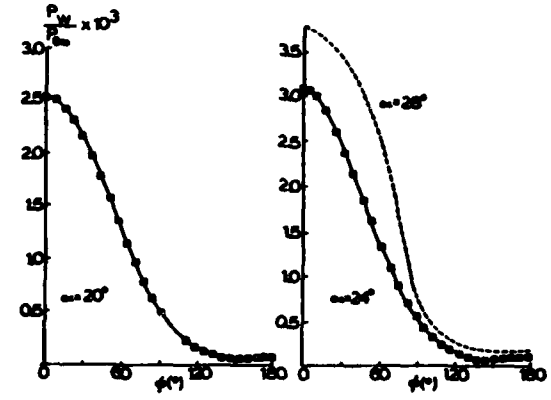

Fig. 6b. Surface Pressure at Large Incidence.

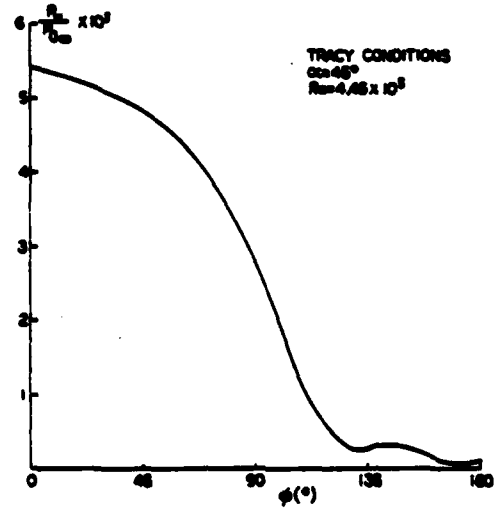

Fig. 6c. Surface Pressure at Very Large Incidence.

the boundary layer, secondary flow separation and the appearance of imbedded shock waves. Near the wind plane, these properties are essentially invariant as is p_0. However, as is seen in the following figures, the secondary flow patterns from the wind plane are extremely complex and include all of the phenomena alluded to previously.

The surface streamline inclination and flow patterns (figures 8, 9 and Table 2) reflect the occurrence of secondary flow separation and for the largest incidence angles a double separation effect is predicted. This phenomena has been seen experimentally in turbulent flows and by Marcillat[9] for laminar flows, but has not been reported in earlier numerical studies. In view of the relatively coarse 51 x 55 uniform grid we reserve comment on the accuracy of the present results; however, the very existence of the converged double separation solutions obtained here is interesting. The primary separation point is relatively insensitive to incidence for large α and is shown in figure 10. As in all earlier calculations, for the present analysis separation first occurs for α : 7° - 8° and the separated regions found by Marcillat[9] for α > 4° are not recovered here. The location of the primary vortex center is depicted in figure 11. The vortex moves away from the surface for increasing α, but appears to asymptote to a fixed location at a given value of

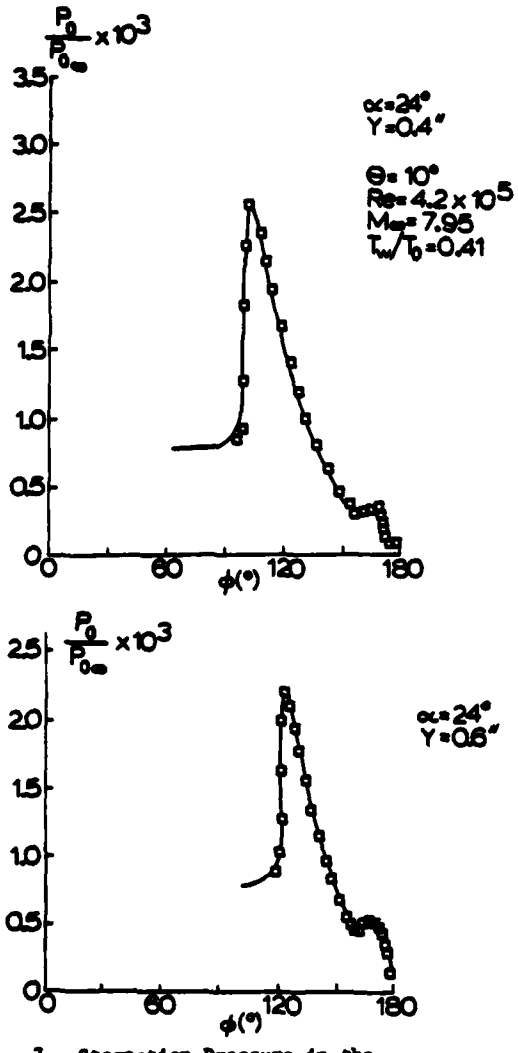

Fig. 7. Stagnation Pressure in the (a) Middle, (b) Vicinity of the Shock Layer - α = 24°.

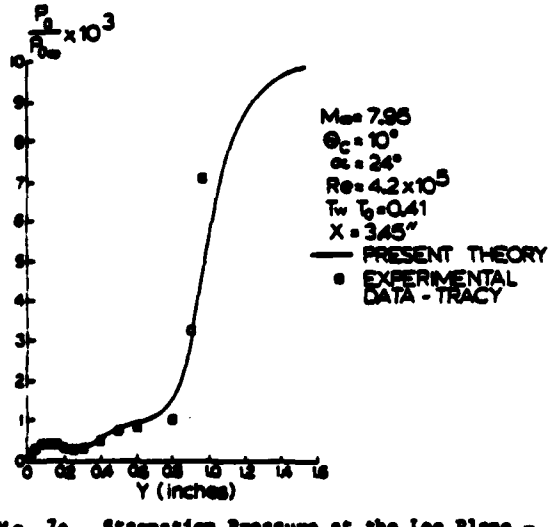

Fig. 7c. Stagnation Pressure at the Lee Plane - α = 24°.

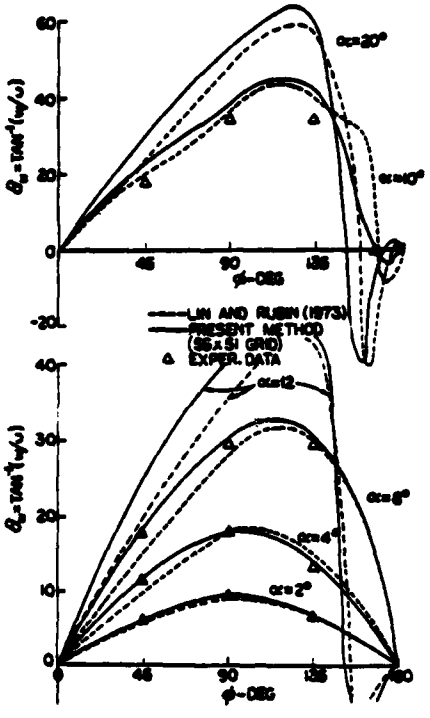

Fig. 8a. Surface Streamline Inclination - Moderate Incidence.

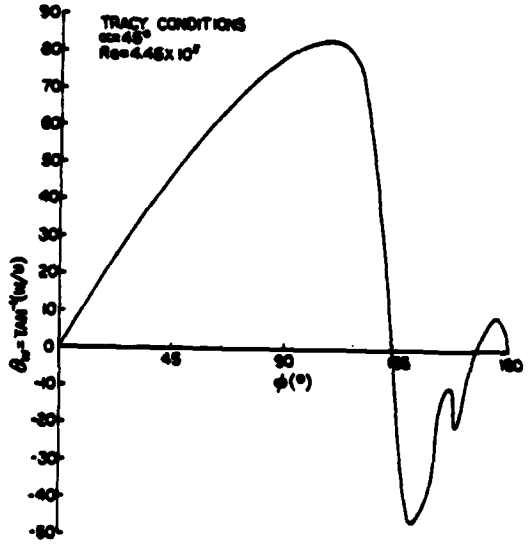

Fig. 8b. Surface Streamline Inclination - Large Incidence.

	ϕ(°)	0	22.5	45	67.5	90	112.5	135	157.5	180
$\alpha = 7°$ $M_\infty = 10$ $\theta = 10°$	JONES (1968) (inviscid)	0	1.732	3.284	4.583	5.517	5.851	5.385	3.502	0
	LIN & RUBIN (1973)	0	1.726	3.291	4.601	5.533	5.870	5.390	3.471	0
	PRESENT METHOD (55 x 51 Grid)	0	1.722	3.288	4.598	5.531	5.872	5.392	3.497	0
$\alpha = 11°$ $M_\infty = 10$ $\theta = 10°$	JONES (1968) (inviscid)	0	2.667	5.333	7.017	9.217	9.300	10.300	7.239	0
	LIN & RUBIN (1973)	0	2.830	5.701	7.889	9.650	10.619	11.090	8.050	0
	PRESENT METHOD (55 x 51 Grid)	0	2.894	5.852	8.113	9.938	10.908	11.486	8.494	0

TABLE 2. SURFACE STREAMLINE INCLINATION, $\tan^{-1}(w_y/u_y)\big|_{y=0}$

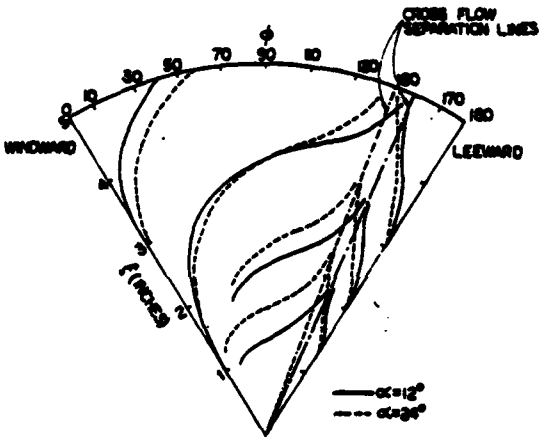

Fig. 9. Surface Streamline Patterns, $\alpha = 12°$, $24°$.

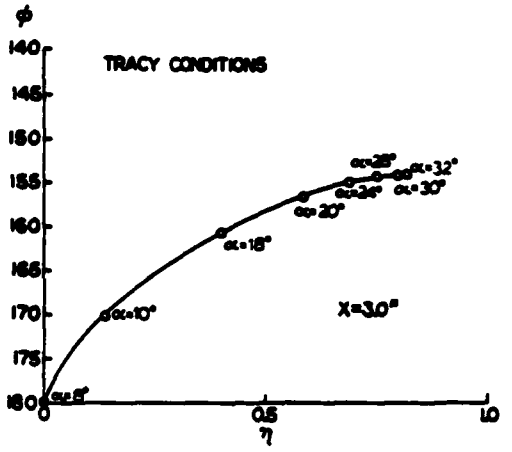

Fig. 11. Primary Vortex Center Location.

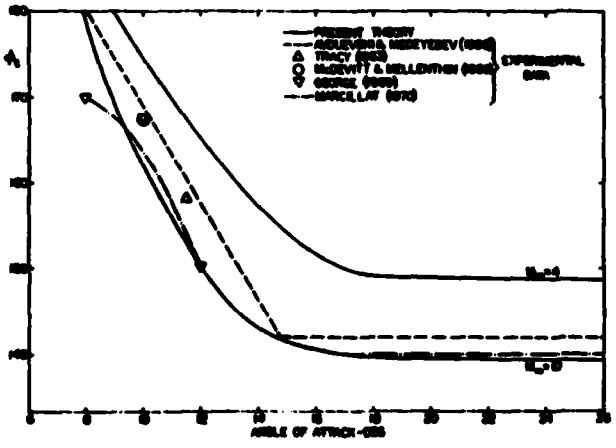

Fig. 10. Primary Separation Point Location.

η relatively close to the shock for $\alpha \geq 30°$. The "inviscid" solution in the outer portion of the shock layer, including the vortex location is approximately independent of ξ and a function only of η and ϕ, i.e., conical flow behavior is observed there.

The boundary and imbedded shock patterns are seen in figures 12a,b,c for several incidence angles. The imbedded shocks increase in strength and the outer shock shape begins to deviate significantly from the near circular pattern at smaller incidence angles. The flow is supersonic over most of the range of ϕ for $\alpha > 12°$.

Finally, for $\alpha = 45°$, the variation of the symmetry plane surface pressure and a qualitative picture of the secondary flow is given in figures 13a,b. The strong imbedded shocks, the double vortex pattern and the apple shape of the outer shock boundary are of particular note. These solutions are converged to the tolerances described earlier; however, the grid may be too coarse to reach a final conclusion on the accuracy of this picture.

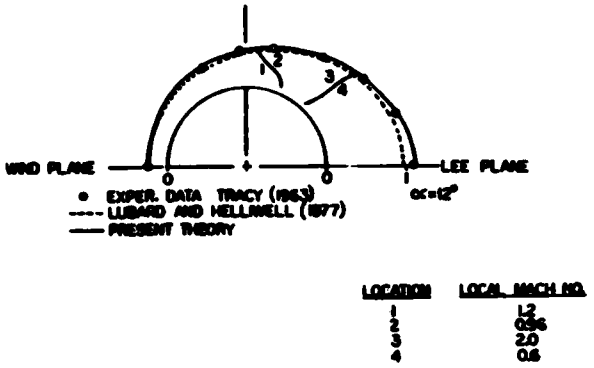

Fig. 12a. Shock Patterns - α = 12°.

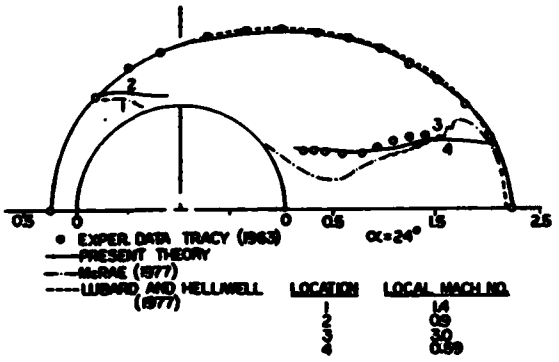

Fig. 12b. Shock Patterns - α = 24°.

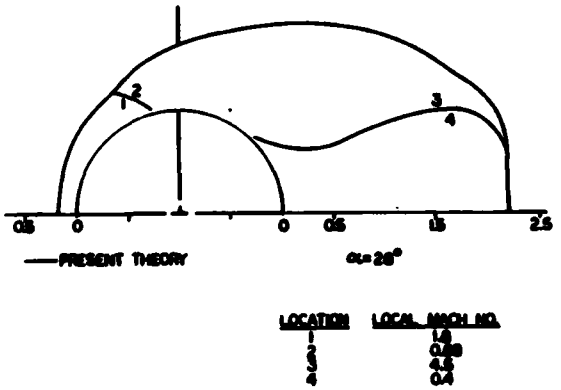

Fig. 12c. Shock Patterns - α = 28°.

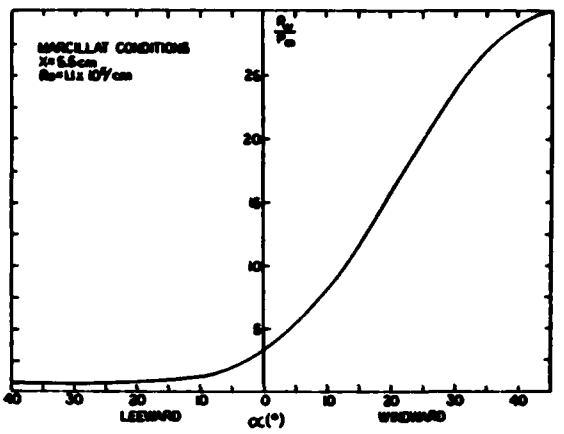

Fig. 13a. Surface Pressure on Symmetry Plane.

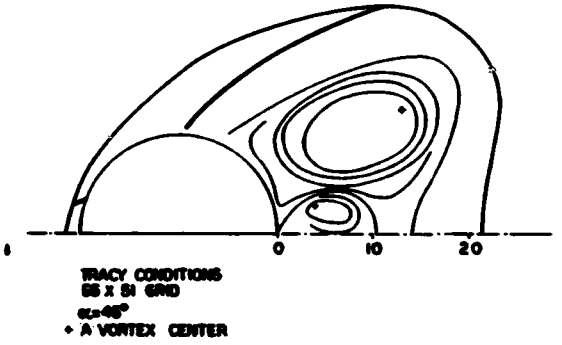

Fig. 13b. Flow Pattern for α = 45°.

In summary, the CSIP procedure described here captures shocks, predicts vortex lift-off, multiple separation regions and complex shock patterns. The possible suppression of departure effects with global iteration and forward p_ξ differencing and the adequacy of single sweep backward differencing and the adequacy of single sweep backward differencing for conical flows with small subsonic viscous layers has been demonstrated. The accuracy of the present solutions for very large incidence remains a question for further study.

Acknowledgement

The author would like to thank Professor P.K. Khosla for many helpful discussions.

This research was supported by the Office of Naval Research under Contract No. N00014-78-0849, Task No. NR 061-258.

References

1. Davis, R.T. and Werle, M.J., (1976), "Numerical Methods for Interacting Boundary Layers," Proc. of the 1976 Heat Transfer and Fluid Mechanics Inst., Stanford University Press.

2. Rubin, S.G., (1981), "A Review of Marching Procedures for Parabolized Navier Stokes Equations," Symposium on Numerical and Physical Aspects of Aerodynamic Flows, California State University, Long Beach, Ca., January 1981, (Proc. by Springer Verlag).

3. Davis, R.T. and Rubin, S.G., (1980), "Non-Navier Stokes Viscous Flow Computations," Computers and Fluids, 8, pp. 101-131.

4. Lin, T.C., Rubin, S.G., Widhoph, G., (1981), "Two Layer Model for Coupled Three Dimensional Viscous and Inviscid Flow Calculations," AIAA 19th Aerospace Sciences Meeting, St. Louis, Mo., January 1981.

5. Rubin, S.G. and Khosla, P.K., (1979), "Navier Stokes Calculations with Coupled Strongly Implicit Method. Part I: Finite Difference Solution," AIAA Paper No. 79-0011. Also, Computers and Fluids, 9, 2, pp. 163-180, 1981.

6. Khosla, P.K. and Rubin, S.G., (1974), "A Diagonally Dominant Second Order Accurate Implicit Scheme," Computers and Fluids, 2, 2, pp. 207-209.

7. Tracy, R.R., (1963), "Hypersonic Flow Over a Yawed Circular Cone," California Institute of Technology, Aeronautical Laboratories, Memorandum No. 69.

8. Rubin, S.G. and Lin, A., (1980), "Marching with the PNS Equations," Proceedings of the 22nd Israel Annual Conference in Aviation and Aeronautics, Tel-Aviv, Israel, pg. 60. (Also, Israel J. of Technology, 18, 1981, in press).

9. Marcillat, J. and Roux, B., (1972), "Experimental and Theoretical Study of Supersonic Flow Over a Yawed Circular Cone," AIAA Journal, 10, 12, pp. 1625-1630. Also: Marcillat, J., Doctoral Thesis, Universite de Province, Marseille, France, July 1970.

10. Schiff, L.B. and Steger, J.L., (1979), "Numerical Simulation of Steady Supersonic Viscous Flow," AIAA Paper No. 79-0130.

11. Lubard, S.C. and Helliwell, W.S., (1975), "An Implicit Method for Three Dimensional Viscous Flow with Application to Cones at Angle of Attack," Computers and Fluids, 3, 1, pp. 83-101.

12. Lin, T.C., and Rubin, S.G., (1973), "Viscous Flow Over a Cone at Moderate Incidenc. I: Hypersonic Tip Region," Computers and Fluids, 1, 1, pp. 37-57.

13. Lin, T.C., and Rubin, S.G., (1973), "Viscous Flow Over a Cone at Moderate Incidence. II: Supersonic Boundary Layer," J. of Fluid Mechanics, 59, 3, pp. 593-620.

14. McRae, D.S., (1976), "A Numerical Study of Supersonic Viscous Cone Flow at High Angle of Attack," AIAA Paper No. 76-77.

15. Avduevsky, V.S. and Medvedev, K.I., (1966), "Investigation of the Laminar Flow Separation on a Cone Under Angle of Attack," Izvestia ANSSR, Fluid and Gas Dynamics, 3, pp. 117-119.

16. Jones, D.J., (1968), "Numerical Solutions of the Flow Field for Conical Bodies in a Supersonic Stream," National Research Council of Canada, NAE LR507.

APPENDIX A

THE CSIP ALGORITHM

$$A_{11_{j,k}} = (Q_3\bar{W}_{2u_{j,k}} - Q_2\bar{W}_{3u_{j,k}})/H$$

$$A_{21_{j,k}} = (R_2\bar{W}_{3u_{j,k}} - R_3\bar{W}_{2u_{j,k}})/H$$

$$B_{11_{j,k}} = (Q_3\bar{W}_{2w_{j,k}} - Q_2\bar{W}_{3w_{j,k}})/H$$

$$B_{21_{j,k}} = (R_2\bar{W}_{3w_{j,k}} - R_3\bar{W}_{2w_{j,k}})/H$$

$$C_{1_{j,k}} = (Q_3\bar{W}_{2v_{j,k}} - Q_2\bar{W}_{2v_{j,k}})/H$$

$$C_{2_{j,k}} = (R_2\bar{W}_{3v_{j,k}} - R_3\bar{W}_{2v_{j,k}})/H$$

$$A_{12_{j,k}} = (Q_3\bar{N}_{2u_{j,k}} - Q_2\bar{N}_{3u_{j,k}})/H$$

$$A_{22_{j,k}} = (R_2\bar{N}_{3u_{j,k}} - R_3\bar{N}_{2u_{j,k}})/H$$

$$B_{12_{j,k}} = (Q_3\bar{N}_{2w_{j,k}} - Q_2\bar{N}_{3w_{j,k}})/H$$

$$B_{22_{j,k}} = (R_2\bar{N}_{3w_{j,k}} - R_3\bar{N}_{2w_{j,k}})/H$$

$$D_{1_{j,k}} = (Q_3\bar{F}_{2_{j,k}} - Q_2\bar{F}_{3_{j,k}})/H$$

$$D_{2_{j,k}} = (R_2\bar{F}_{3_{j,k}} - R_3\bar{F}_{2_{j,k}})/H$$

$$H = R_2Q_3 - R_3Q_2$$

For $\ell = 2, 3$ we define:

$$R_\ell = -(P_{\ell_u} + \bar{P}_{\ell_v}\bar{P}_{1u} + E_{\ell_u}A_{11_{j+1,k}} + E_{\ell_w}A_{21_{j+1,k}} + S_{\ell_u}A_{12_{j,k-1}} + S_{\ell_w}A_{22_{j,k-1}})$$

$$Q_\ell = -(P_{\ell_w} + \bar{P}_{\ell_v}\bar{P}_{1w} + E_{\ell_u}B_{11_{j+1,k}} + E_{\ell_w}B_{21_{j+1,k}} + S_{\ell_u}B_{12_{j,k-1}} + S_{\ell_w}B_{22_{j,k-1}})$$

$$\bar{F}_{\ell_v} = F_{\ell_v} + E_{\ell_u} C1_{j+1,k} + E_{\ell_w} C2_{j+1,k}$$

$$\bar{F}_{1u} = F_{1u} + S_{1w} A22_{j,k-1}$$

$$\bar{F}_{1w} = F_{1w} + S_{1w} B22_{j,k-1}$$

$$\bar{W}_{\ell_{u_{j,k}}} = W_{\ell_{u_{j,k}}} + W_{1u_{j,k}} \bar{F}_{\ell_v}$$

$$\bar{W}_{\ell_{w_{j,k}}} = W_{\ell_{w_{j,k}}} + W_{1w_{j,k}} \bar{F}_{\ell_v}$$

$$\bar{H}_{\ell_{u_{j,k}}} = H_{\ell_{u_{k,k}}} + H_{1u_{j,k}} \bar{F}_{\ell_v}$$

$$\bar{H}_{\ell_{w_{j,k}}} = H_{\ell_{w_{j,k}}} + H_{1w_{j,k}} \bar{F}_{\ell_v}$$

$$\bar{F}_{\ell_{j,k}} = F_{\ell_{j,k}} + \bar{F}_{\ell_v} \bar{F}_{1_{j,k}} + E_{\ell_u} (A12_{j+1,k} U_{j+1,k+1}$$

$$+ B12_{j+1,k} W_{j+1,k+1} + D1_{j+1,k})$$

$$+ E_{\ell_w} (A22_{j+1,k} U_{j+1,k+1} + B22_{j+1,k} W_{j+1,k+1}$$

$$+ D2_{j+1,k}) + S_{\ell_u} (A11_{j,k-1} U_{j-1,k-1}$$

$$+ B11_{j,k-1} W_{j-1,k-1} + D1_{j,k-1}$$

$$+ C1_{j,k-1} V_{j-1,k-1})$$

$$+ S_{\ell_w} (A21_{j,k-1} U_{j-1,k-1} + B21_{j,k-1} W_{j-1,k-1}$$

$$+ D2_{j,k-1} + C2_{j,k-1} V_{j-1,k-1}$$

$$\bar{F}_{1_{j,k}} = F_{1_{j,k}} + S_{1w} (A21_{j,k-1} U_{j-1,k-1}$$

$$+ B21_{j,k-1} V_{j-1,k-1} + C2_{j,k-1} V_{j-1,k-1}$$

$$+ D2_{j,k-1})$$

APPENDIX B

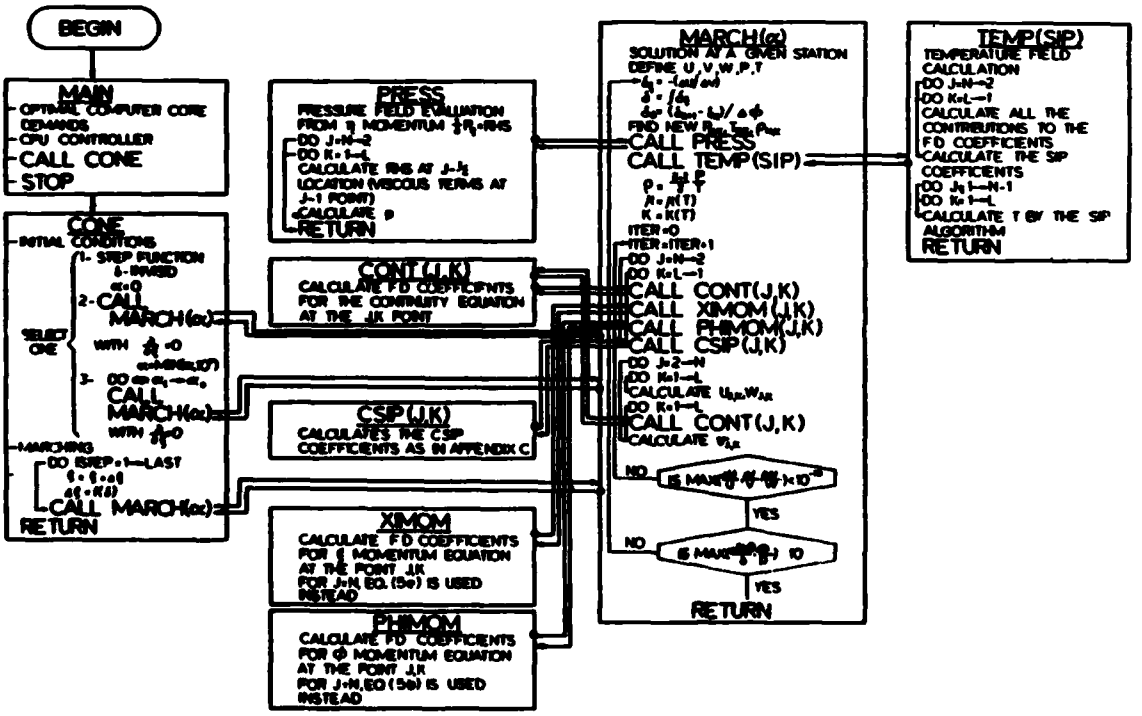

$$\bar{F}_{\ell_v} = F_{\ell_v} + E_{\ell_u} C_{1_{j+1,k}} + E_{\ell_w} C_{2_{j+1,k}}$$

$$\bar{F}_{1u} = F_{1u} + S_{1w} A_{22_{j,k-1}}$$

$$\bar{F}_{1w} = F_{1w} + S_{1w} B_{22_{j,k-1}}$$

$$\bar{W}_{\ell_{u_{j,k}}} = W_{\ell_{u_{j,k}}} + W_{1u_{j,k}} \bar{F}_{\ell_v}$$

$$\bar{W}_{\ell_{w_{j,k}}} = W_{\ell_{w_{j,k}}} + W_{1w_{j,k}} \bar{F}_{\ell_v}$$

$$\bar{H}_{\ell_{u_{j,k}}} = H_{\ell_{u_{k,k}}} + H_{1u_{j,k}} \bar{F}_{\ell_v}$$

$$\bar{H}_{\ell_{w_{j,k}}} = H_{\ell_{w_{j,k}}} + H_{1w_{j,k}} \bar{F}_{\ell_v}$$

$$\bar{F}_{\ell_{j,k}} = F_{\ell_{j,k}} + \bar{F}_{\ell_v} \bar{F}_{1_{j,k}} + E_{\ell_u} (A_{12_{j+1,k}} U_{j+1,k+1}$$

$$+ B_{12_{j+1,k}} W_{j+1,k+1} + D_{1_{j+1,k}})$$

$$+ E_{\ell_w} (A_{22_{j+1,k}} U_{j+1,k+1} + B_{22_{j+1,k}} W_{j+1,k+1}$$

$$+ D_{2_{j+1,k}}) + S_{\ell_u} (A_{11_{j,k-1}} U_{j-1,k-1}$$

$$+ B_{11_{j,k-1}} W_{j-1,k-1} + D_{1_{j,k-1}}$$

$$+ C_{1_{j,k-1}} V_{j-1,k-1})$$

$$+ S_{\ell_w} (A_{21_{j,k-1}} U_{j-1,k-1} + B_{21_{j,k-1}} W_{j-1,k-1}$$

$$+ D_{2_{j,k-1}} + C_{2_{j,k-1}} V_{j-1,k-1}$$

$$\bar{F}_{1_{j,k}} = F_{1_{j,k}} + S_{1w} (A_{21_{j,k-1}} U_{j-1,k-1}$$

$$+ B_{21_{j,k-1}} V_{j-1,k-1} + C_{2_{j,k-1}} V_{j-1,k-1}$$

$$+ D_{2_{j,k-1}})$$

APPENDIX B

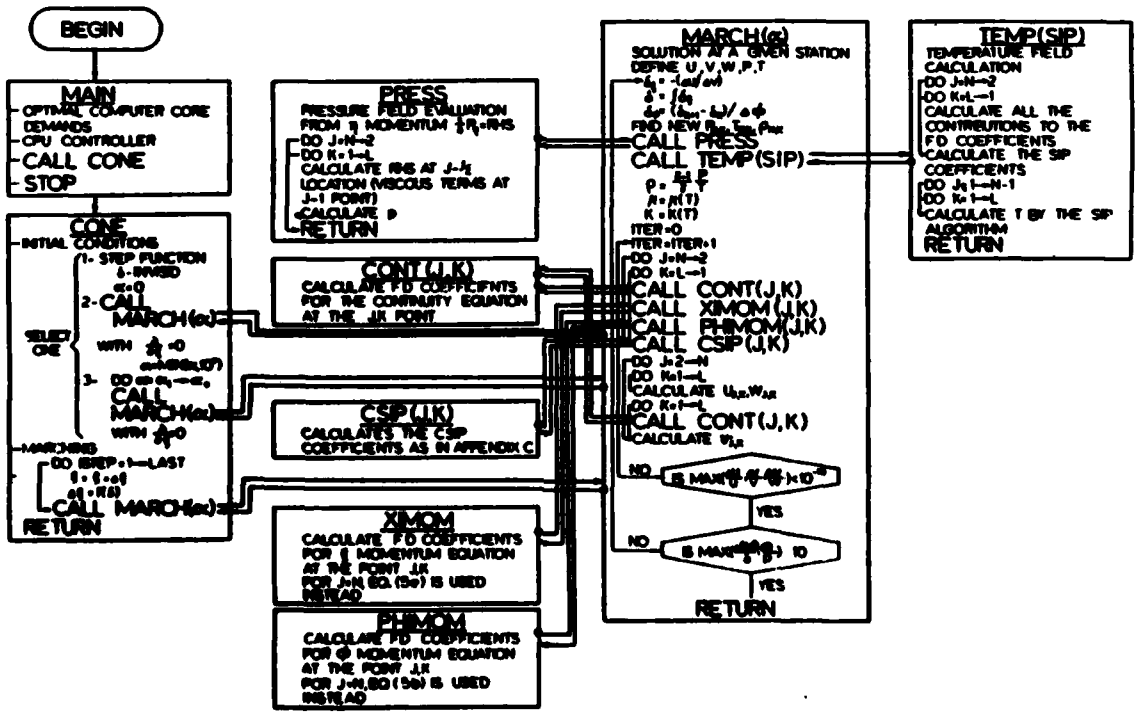

UNCLASSIFIED

SECURITY CLASSIFICATION OF THIS PAGE (When Data Entered)

REPORT DOCUMENTATION PAGE

READ INSTRUCTIONS BEFORE COMPLETING FORM

1. REPORT NUMBER: AIAA PAPER NO. 81-0192
2. GOVT ACCESSION NO.: AD-A096 232
3. RECIPIENT'S CATALOG NUMBER:

(6) 4. TITLE (and Subtitle): THREE-DIMENSIONAL SUPERSONIC VISCOUS FLOW OVER A CONE AT INCIDENCE

5. TYPE OF REPORT & PERIOD COVERED: INTERIM

6. PERFORMING ORG. REPORT NUMBER:

(10) 7. AUTHOR(s): A. LIN, S.G. RUBIN

8. CONTRACT OR GRANT NUMBER(s): N00014-79-C-0849

9. PERFORMING ORGANIZATION NAME AND ADDRESS: UNIVERSITY OF CINCINNATI, DEPARTMENT OF AEROSPACE ENG. & APPLIED MECHANICS, CINCINNATI, OH 45221 / 410677

10. PROGRAM ELEMENT, PROJECT, TASK AREA & WORK UNIT NUMBERS: NR 061-258

11. CONTROLLING OFFICE NAME AND ADDRESS: DEPARTMENT OF THE NAVY, OFFICE OF NAVAL RESEARCH, ARLINGTON, VIRGINIA 22217

12. REPORT DATE: (11) JAN 1981 (13) 74

13. NUMBER OF PAGES: 12

14. MONITORING AGENCY NAME & ADDRESS (if different from Controlling Office): (15) N00014-79-C-0849

15. SECURITY CLASS. (of this report): UNCLASSIFIED

15a. DECLASSIFICATION/DOWNGRADING SCHEDULE:

16. DISTRIBUTION STATEMENT (of this Report)

APPROVED FOR PUBLIC RELEASE: DISTRIBUTION UNLIMITED

17. DISTRIBUTION STATEMENT (of the abstract entered in Block 20, if different from Report)

18. SUPPLEMENTARY NOTES

19. KEY WORDS (Continue on reverse side if necessary and identify by block number)

CONE FLOW
SUPERSONIC
LAMINAR
COUPLED STRONGLY IMPLICIT
BOUNDARY LAYER-LIKE
PARABOLIZFD NAVIER-STOKES
LARGE INCIDENCE

Accession For
NTIS GRA&I
DTIC TAB
Unannounced
Justification
By
Distribution/
Availability Codes
Dist
A

20. ABSTRACT (Continue on reverse side if necessary and identify by block number)

The viscous supersonic flow over a sharp cone at incidence is examined numerically with a coupled strongly implicit algorithm for the properties in the plane normal to the cone axis. The Navier-Stokes equations are considered in a boundary layer-like or parabolized manner and global relaxation is considered for the pressure interaction. It is shown that departure effects can be effectively eliminated by forward differencing for the axial pressure gradient. Moreover, this approximation retains the implicit free pressure interaction required for geometries where axial flow separation is possible.

DD FORM 1 JAN 73 1473 EDITION OF 1 NOV 65 IS OBSOLETE

UNCLASSIFIED 410677 slt

SECURITY CLASSIFICATION OF THIS PAGE (When Data Entered)

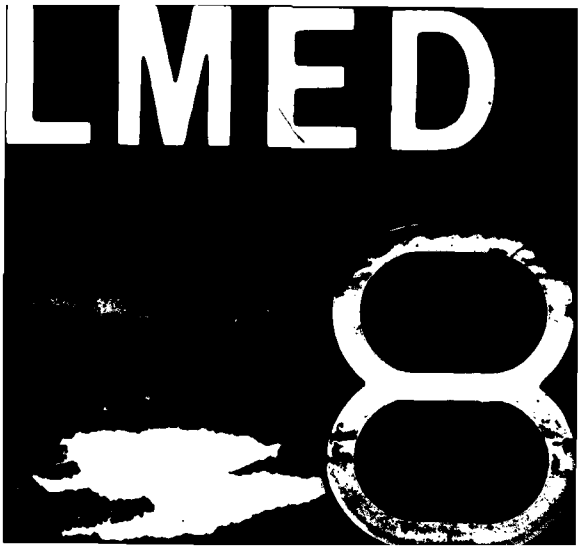
LMED